Impressão por escrita direta utilizando binder reativo baseado na resina de Pechini para a obtenção de suportes catalíticos de SnO_2 de fase pura

Pechini-based reactive-binder ceramic suspension for direct ink writing of phase-pure structured SnO_2 catalyst supports

Carolina Mendes Furlan Ferreira[1], Anderson Luis Barbosa[2], Cátia Alexandra Podence Alves[2], Andre Luiz da Silva[2], Douglas Gouvêa[2], Bruno Ramos[1,2]

Microfluidic & Photoelectrocatalytic Engineering Lab, Department of Chemical Engineering, Centro Universitario FEI, Av. Humberto de A. Castelo Branco 3972, São Bernardo do Campo, Brazil, 09850-901

Laboratory of Ceramics Processes, Departament of Metallurgic and Materials Engineering, Escola Politécnica, Universidade de São Paulo, Av. Prof. Mello Moraes 2463. São Paulo, Brazil, 05508-900

brunoramos@fei.edu.br

Resumo

O óxido de estanho (SnO_2) é um óxido metálico quimicamente estável e ativo em processos oxirredutivos, amplamente utilizado como suporte catalítico em reações heterogêneas, detecção de gases e aplicações relacionadas à energia. Neste trabalho, apresentamos uma abordagem inovadora para a manufatura aditiva de suportes catalíticos estruturados de SnO_2 por extrusão de pasta cerâmica (DIW), utilizando um ligante reativo derivado do método de Pechini. A formulação da pasta combina pó comercial de SnO_2 com um complexo polimerizável de estanho, ácido cítrico e etilenoglicol, que atua simultaneamente como modificador reológico e precursor metálico. Essa dupla função elimina a necessidade de agentes plasticizantes inertes ou ligantes à base de óxidos não-nativos. A pasta resultante apresenta propriedades viscoelásticas adequadas para conformação por extrusão e, após calcinação, o ligante se decompõe e se converte em SnO_2, complementando a carga sólida inicial. As peças sinterizadas mantêm sua integridade geométrica, tornando-se ideais para aplicações catalíticas que exigem alta estabilidade térmica e química. Essa estratégia de ligante reativo oferece uma rota simples, escalável e quimicamente limpa para a fabricação de componentes estruturados à base de óxidos metálicos, com potencial de aplicação em sistemas monometálicos ou óxidos mistos.

palavras-chave: Óxido de estanho, Impressão 3D, Ligante reativo

Abstract

Tin oxide (SnO_2) is a chemically stable, redox-active metal oxide widely employed as a catalyst support in heterogeneous reactions, gas sensing, and energy-related applications. Here, we present a novel approach for the additive manufacturing of structured SnO_2 catalyst supports via direct ink writing (DIW), utilising a Pechini-derived reactive binder. The ink formulation combines commercial SnO_2 powder with a polymerisable complex of tin, citric acid, and ethylene glycol, which functions both as a rheological modifier and as a metal oxide precursor. This dual role eliminates the need for inert thickeners or non-native oxide binders. The resulting paste exhibits suitable viscoelastic properties for extrusion-based shaping and, upon calcination, the binder decomposes and converts to SnO_2, complementing the original solid loading. The sintered pieces retain their geometric integrity, rendering them ideal for catalytic applications requiring high thermal and chemical stability. This reactive-binder strategy offers a straightforward, scalable, and compositionally clean route to structured metal oxide components, with potential applicability to other single or mixed oxide systems.

Key-words: Tin oxide, Direct Ink Writing, reactive binder

1. INTRODUCTION

Energy Transition is possibly one of the biggest challenges that we face as a society in the 21st century. Driven by extreme climate events attributed to rising atmospheric CO_2 levels, promoted by the extensive use of oil- and coal-derived combustion, this new transition pushes us to find alternative energy systems and routes to produce materials essential for our modern society. Overcoming this challenge requires a collective and multidisciplinary effort, of which the design of robust, efficient and sustainable catalysts is a major example.

Recent works from our group have explored the synthesis and application of metal oxides in processes relevant to Energy Transition, including the conversion of CO_2 to value-added fuels [1], and the synthesis of ammonia from dissolved N_2 in ambient conditions [2], where they act as catalysts. In earlier development stages, the catalysts are typically synthesized in powder form, but for achieving higher technological readiness levels and facilitate out-scaling, having them in easily-handled forms is essential. In practical large-scale applications, solid catalysts are typically shaped into or fixed onto larger particles, such as pellets or other geometrical fillings, which are then inserted on reaction vessels. These pieces of equipment are intended to promote optimal contact between the reactants, usually fluids, and the catalysts; and the geometry of the support is designed to facilitate this process while also controlling the pressure drop through the equipment, reducing the energy demand. To fix the catalysts onto supporting materials, synthesis methods such as ultrasonic spray [3], jet-inking [4], spin-coating [5] or dip-coating [6] can be used. While these methods are well established, an active research area is that of tailoring the support properties and geometry.

Among the various catalyst supports reported in the literature, ceramic materials are more frequently employed due to their high thermal and chemical stability, mechanical robustness, and resistance to sintering under harsh reaction conditions. In addition, their surface chemistry can be tuned to optimize catalyst-support interactions, enhancing the dispersion, stability, and activity of the active phase. The specialized literature has shown that the nature of the support affects the performance of the catalysts, so tailoring its composition – particularly avoiding the presence of unwanted species, especially metallic ions – is a key aspect of materials processing. Studies report that supports with high surface area and tailored porosity, such as mesoporous metal oxides, promote uniform dispersion, stabilize nanoparticle size (often below 6 nanometres), and generate active metal-support interfaces that boost turnover frequencies by orders of magnitude in reactions like carbon monoxide oxidation [7]. In addition, supports that provide oxygen vacancies, specific redox states, and controlled surface chemistry (for example, cerium dioxide and titanium dioxide) enhance oxygen activation and strengthen metal-support bonding. These features are able to improve reaction rates and also selectivity and durability in a range of industrial processes, including electrocatalysis, preferential oxidation, and steam reforming [8].

Several routes have been developed to produce ceramic catalyst supports with tailored composition, morphology, and surface chemistry. Advanced additive manufacturing techniques, such as extrusion-based 3D printing (*Direct Ink Writing*) and stereolithography, allow the direct fabrication of structured supports with customised geometries, optimised flow channels, and hierarchical porosity [9]. These methods facilitate the incorporation of specific design parameters from the early stages of fabrication.

Conventional ceramic processing relies heavily on polymeric binders to impart plasticity, cohesion, and shape retention during forming. These additives, however, are transient and must be removed prior to densification, often through thermal debinding, a step that can introduce defects such as cracking, carbon retention, or anisotropic shrinkage if not carefully controlled [10]. Such challenges underscore the limitations of inert binders, which serve only as processing aids and contribute no functional role to the final ceramic body. In contrast, reactive binders offer a transformative alternative: they simultaneously tailor rheology during shaping and convert into the target oxide upon calcination, thus eliminating foreign species and contributing to the final solid loading [11]. Recent developments have demonstrated their potential to yield phase-pure ceramic components while simplifying debinding and improving microstructural integrity [12,13]. Building on this approach, we previously reported a method for preparing TiO_2 structures by direct ink writing without the use of inorganic binders, thereby avoiding the incorporation of unwanted metal cations [12], and here we extend this methodology to SnO_2, a material valued for its thermal and chemical stability, tunable electronic structure, strong metal–support interactions, and morphological flexibility. These properties make SnO_2 particularly attractive as a support for metals in electrocatalytic processes [14], especially under oxidising or high-temperature conditions, NOx reduction [15], and biocatalysis [16], among others.

2. METHODOLOGY

2.1 Materials

Tin(IV) oxide (SnO_2, Balestro Inc.) was used as the primary ceramic phase. Tin oxalate (SnC_2O_4, ≥98 %, Sigma–Aldrich) was employed as the inorganic precursor in the preparation of the Pechini-type polymeric resin. Citric acid (≥99.5 %, Synth), monoethylene glycol (≥99.0 %, Neon), nitric acid (65%, Synth) and deionized water were used for preparing the resin. All reagents were used without further purification.

2.2 Formulation of the ceramic paste

The extrudable SnO_2 ceramic paste was prepared by mixing a polymeric resin at 1500 rpm with dried SnO_2 powder, which was gradually incorporated to achieve the desired solid loading, followed by mixing at 2500 rpm for 60 s to ensure homogeneity. The compositions were adjusted to obtain different ratios of solids loading, 76.02%, 74.37%, 75.00% and 72.50% (SnO_2-1, SnO_2-2, SnO_2-3, and SnO_2-4, respectively).

The polymeric resin, containing a precursor for *in-situ* formation of SnO_2 nanoparticles, was prepared via a modified Pechini process [17]. Briefly, monoethylene glycol was heated to approximately 70 °C together with citric acid, using a magnetic stirrer. Once a homogeneous mixture was obtained, i.e., a clear, transparent solution, the sample was kept for 30 minutes in the polymerization process at 120 °C. Meanwhile, the tin oxalate solution was stirred with 23 wt% diluted nitric acid for about 1 hour in order to convert the oxidation state to +4, needed to form SnO_2 during de calcination process. Finally, the tin oxalate was slowly added to the monoethylene glycol and citric acid mixture at 120 °C, while being stirred at a constant speed with the aid of a magnetic stirrer for 30 minutes. The SnO_2 content (7.75%) of the resin was determined by calcining a resin sample at 900 °C for 5 h in air, and its water content was calculated by thermogravimetry (37.8 ± 2.2%) upon drying paste samples at 120 °C for 48 hours.

2.3 Direct ink writing

The pastes were printed using a cartesian-type 3D printer (DuraPrinter C02, Duracer) equipped with a piston-driven reservoir feeding an Auger extrusion system. Printing was carried out at a reservoir pressure of 3 bar through a 1.2 mm nozzle. The slicing was performed in Ultimaker Cura with the following parameters: layer height = 0.8 mm; initial layer height = 0.5 mm; line width = 1.2 mm; flow = 200 %; printing speed = 15 mm s^{-1}; travel speed = 30 mm s^{-1}; spiralized outer contour mode = on. No top/bottom layers were printed to obtain hollow-walled geometries. The printed test geometry was a 40 x 40 mm hollow cylinder, designed to evaluate the shape fidelity and self-support capability of the paste. After printing, samples were dried at ambient conditions for 48 h and calcined in air at 500 °C (2 °C min^{-1}) for 5 h.

2.4 Analyses

The X-ray diffraction patterns (XRD) were obtained using an X'Pert-MPD (Philips) diffractometer with Cu Kα radiation, operated at 45 kV and 40 mA. The step size was set at 0.02° 2θ per second over the 10-90° 2θ range. The crystallite sizes and the lattice parameters were calculated by the Rietveld analysis using the X'Pert Highscore software with $MgAl_2O_4$ as the standard. The powder density was measured using a Micromeritics AccuPyc II 1340 He gas pycnometer after 200 purges for degassing. The specific surface area was determined by nitrogen gas adsorption at 77 K (Micromeritics Gemini III 2375), according to the Brunauer-Emmett-Teller (BET) method. The samples were degassed at 250 °C for ~12 h before the experiment using a VacPrep 061 (Micromeritics). Diffuse reflectance infrared Fourier transform (DRIFT) spectroscopy was performed using a Nicolet iS50 spectrometer to identify the functional groups adsorbed on powder. DRIFT spectra were recorded in the range of 400-4000 cm^{-1}. The rheological behaviour was measured using a HAAKE MARS 60 rheometer (Thermo Fisher Scientific) with 35 mm parallel plates and a 1 mm gap at 23 °C, following a pre-shear at 5 s^{-1} for 30 s and a shear rate sweep from 1 to 30 s^{-1} and back to 1 s^{-1} to obtain flow curves and hysteresis loops.

3. RESULTS AND DISCUSSION

3.1 Preparation of the tin oxide resin

The resin was prepared as reported in section 2.2. The resulting material was a viscous, translucid yellowish liquid. Upon calcination, a white powder was obtained, with a yield of 7.75% (g SnO_2 / 100 g of resin). This powder was investigated by X-ray diffraction (XRD), as shown in **Figure 1**. Broad diffraction peaks are observed, which are characteristic of nanosized crystallites. Cassiterite (JCPDS card no. 41-1445) was the only phase identified.

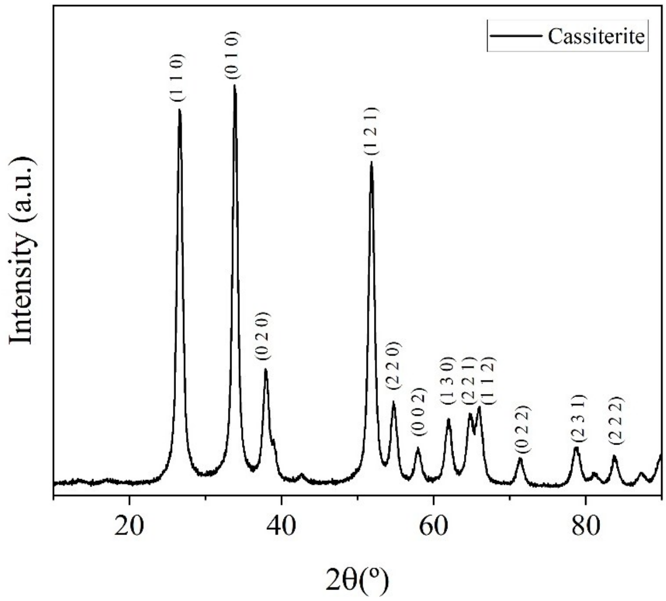

Figure 1. *XRD pattern of SnO2 nanopowders obtained upon calcination of the resin.*

The average crystallite size and lattice parameters of the nanopowders were calculated after Rietveld refinement of XRD data. The estimated crystallite size was 10.71 nm, while the refined lattice parameters were a = b = 4.7355 Å and c = 3.1835 Å. These values are in good agreement with previously reported data in the literature [18,19]. The samples exhibited a surface area of 47.2 ± 0.1 m²/g, consistent with literature values for SnO_2 nanopowders [ref], and a density of 6.02 ± 0.03 g/cm³, lower than that of bulk SnO_2 (6.91–6.95 g/cm³) [ref], due to the nanoscale dimensions and porosity of the powders. DRIFTS spectrum of the prepared SnO_2 is given in **Figure 2**.

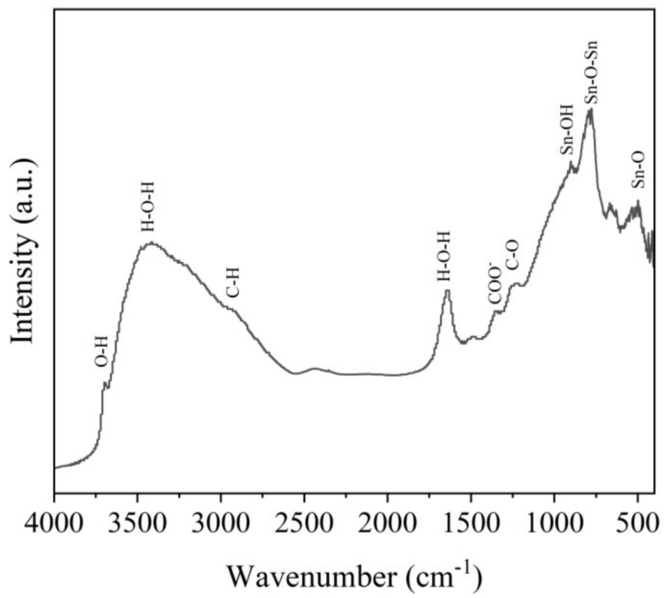

Figure 2. *DRIFTS spectrum of SnO_2 nanopowder.*

The IR diffuse reflectance spectrum shows a broad band at ~3400 cm^{-1} assigned to O–H stretching vibrations of surface hydroxyl groups and adsorbed water, while the band at ~1630 cm^{-1} corresponds to H–O–H bending. Weak absorptions around 2920 cm^{-1} are attributed to C–H stretching, indicating residual organic species from the synthesis. The band at ~1360 cm^{-1} is associated with COO^- stretching, and a signal in ~ 1240 cm^{-1} region corresponds to C–O vibrations, suggesting adsorbed carbonate. In the low wavenumber region, characteristic bands of Sn–O and Sn–O–Sn vibrations are observed at ~520 and ~780 cm^{-1}, confirming the formation of the Sn–O lattice.

3.2 Paste rheology

The rheological properties of the SnO_2-loaded pastes were evaluated to assess their suitability for 3D printing by direct ink writing (DIW), using SH94.4, a material with exemplary extrudable properties, as a benchmark. As shown in the flow curves in **Figure 3A**, all formulated pastes exhibited the essential pseudoplastic (shear-thinning) behaviour required for extrusion, where viscosity decreases under shear increase, enabling flow through a nozzle. This phenomenon is attributed to the alignment of polymer binder chains and the breakdown of particle agglomerates under stress [12,20].

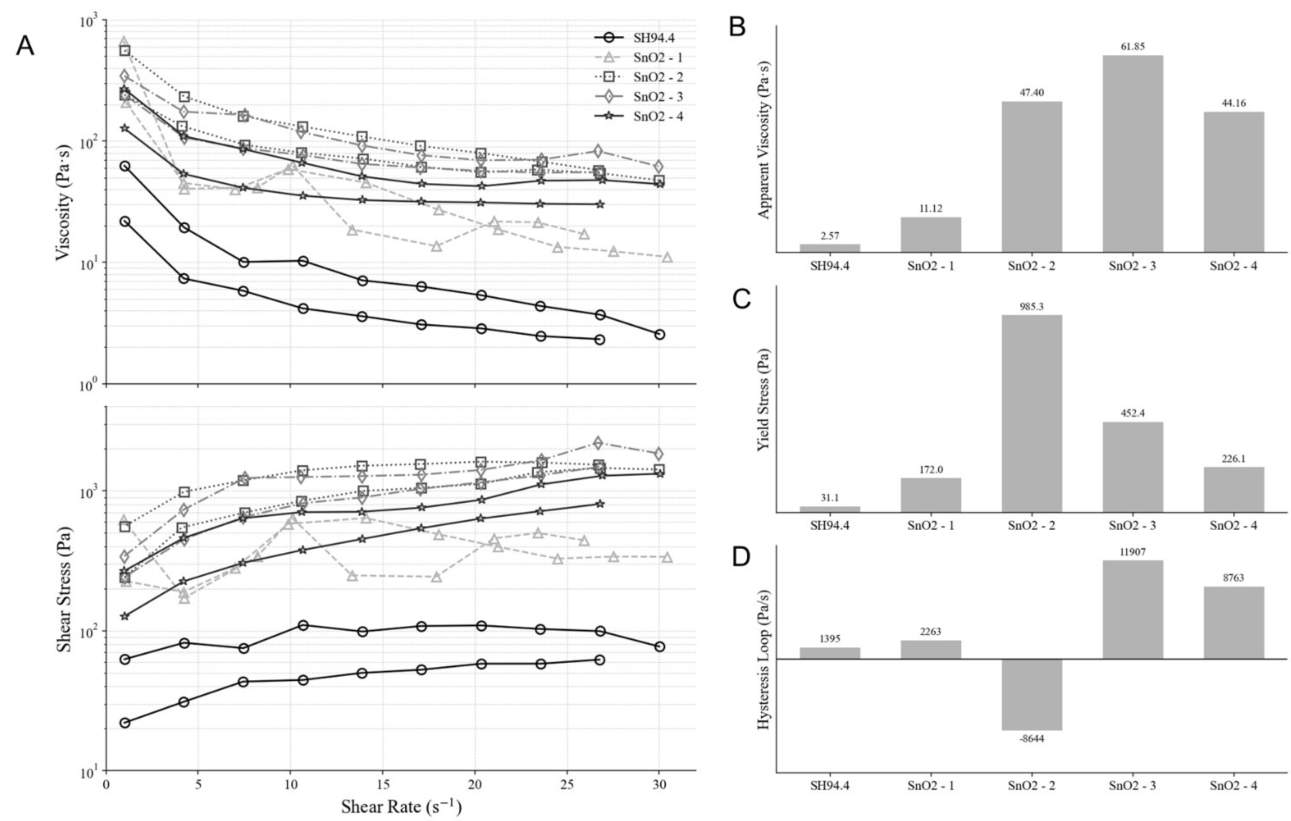

***Figure 3**. Rheological properties of the formulated ceramic pastes. (A) Full hysteresis loops for Viscosity and Shear Stress plotted against Shear Rate, confirming the pseudoplastic (shear-thinning) nature of all samples. The derived quantitative parameters are summarized for (B) Apparent Viscosity, (C) Yield Stress, and (D) Hysteresis Loop area. The data highlights the unique anti-thixotropic behaviour and high yield stress of the SnO_2-2 formulation.*

A detailed analysis of the rheological parameters, summarized in **Figure 3B-D**, reveals critical performance differences. While the SH94.4 benchmark possesses a modest yield stress (31.1 Pa, **Figure 3C**), all SnO_2-loaded pastes offered a substantial increase. This is crucial for ensuring the shape fidelity of printed structures, as a sufficiently high yield stress allows filaments to support their own weight and the weight of subsequent layers [21]. However, an optimal rheological window exists, as an excessively high yield stress can prevent proper filament flow, leading to detrimental inter-filament porosity in the final part [13]. The most significant differentiator for DIW performance, however, is the time-dependent viscosity recovery (or *self-healing* *capacity*), quantified by the hysteresis loop area (**Figure 3D**) [22]. The 75% solid loading paste (SnO_2-3) displayed strong thixotropic behaviour (11,907 Pa/s), far exceeding that of SH94.4. This indicates a much faster structural recovery post-extrusion, ideal for preventing filament collapse during layer-by-layer construction.

In stark contrast, the 74.37% paste (SnO_2-2) exhibited pronounced negative thixotropic behaviour, evident from its large negative hysteresis value in Figure 3d. This property indicates slower structural recovery of the paste, which can affect the shape retention of the extruded filament and ability of self-support [20,23,24]. These findings resonate with recent meta-analyses of DIW ink design, which define a narrow "*rheological window*" where extrudability and shape fidelity coexist [13]. Barbosa et al. (2025) [12] further demonstrated that Pechini-derived polymeric binders can act dually as organic and inorganic binders, improving rheological control while contributing to oxide formation upon calcination. The present SnO_2 pastes extend this concept, evidencing those reactive binders improve viscoelastic properties and also yield a phase-pure oxide without extraneous cations, an advantage over conventional inert polymer additives.

3.3 Extrusion evaluation

Following the rheological characterization, the practical printability of each paste was evaluated using a direct ink writing (DIW) system with a 410 µm nozzle and a maximum dispensing pressure of 3 bar. The test body was a thin-walled regular cylinder, as shown in **Figure 4A**. The extrusion trials were performed to validate the rheological predictions and identify a formulation capable of forming stable, self-supporting structures.

The initial screening revealed a critical processing challenge. The pastes with higher solid loadings, 76.02% (SnO_2-1), 75.00% (SnO_2-3), and 74.37% (SnO_2-2), could not be extruded as they required a pressure exceeding the 3 bar limit, a result consistent with their high yield stresses (**Figure 3C**). Conversely, the paste with the lowest solid loading of 72.50% (SnO_2-4) was easily extrudable. However, due to its insufficient yield stress (226.1 Pa), the printed lines were not self-standing and exhibited immediate slumping, resulting in a collapsed structure as shown in **Figure 4C**. This confirmed that none of the initial formulations resided within the required rheological window for successful DIW. This behaviour parallels reports on alumina and titania DIW systems, where insufficient yield stress compromises mechanical stability of green bodies [21].

Given that the SnO_2-3 formulation possessed the highest yield stress and therefore the greatest potential for shape retention, a slight modification was made to this paste to reduce its flow resistance just enough to enable extrusion, resulting in SnO_2-2. This optimized paste was successfully printed at approximately 2.9 bar, demonstrating both smooth deposition and excellent self-supporting properties. A thin cylindrical body structure was successfully fabricated using this formulation, as shown in the as-printed "green body" in **Figure 4D**.

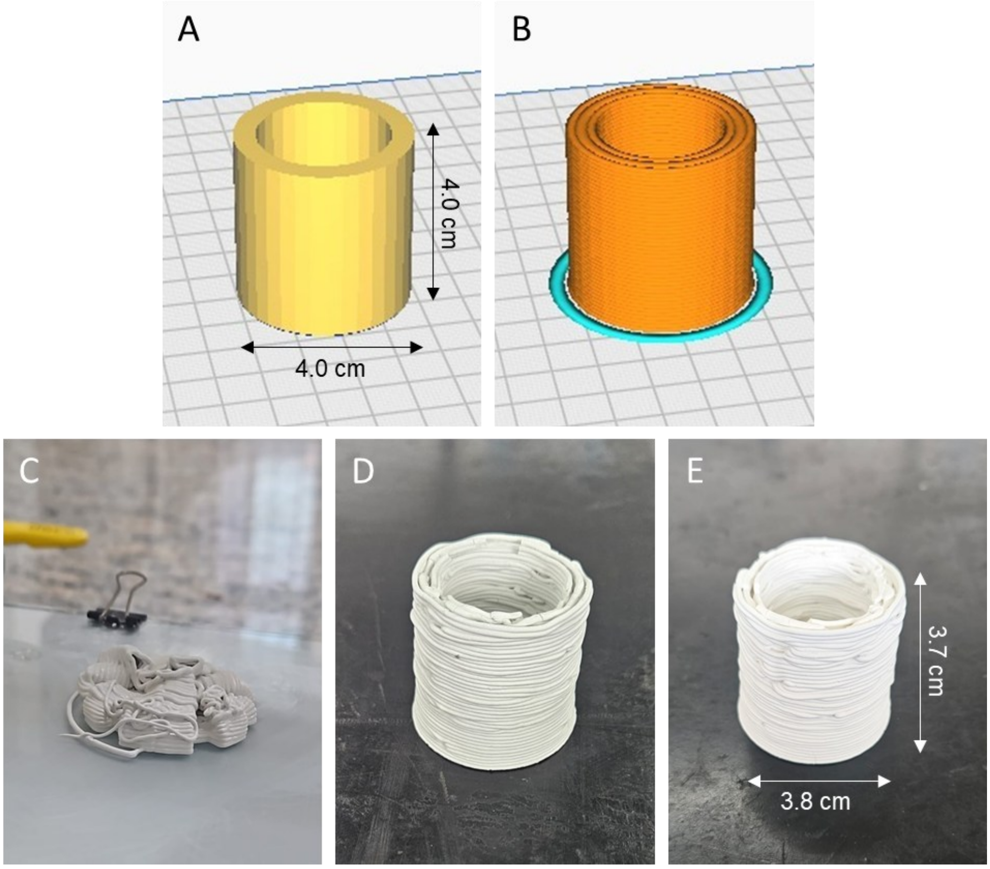

Figure 4. *Direct ink writing (DIW) of SnO_2 structures showing: (a) the digital CAD model of the target geometry; (b) the sliced digital model, illustrating the G-code toolpath; (c) structural collapse of the extruded SnO_2-4 paste; (d) the self-supporting as-printed green body fabricated using the optimal SnO_2-2 paste; and (e) the final SnO_2 ceramic cylinder after calcination.*

Finally, to obtain the dense ceramic component, the successfully printed green body was subjected to a calcination process. This thermal treatment removed the organic binder and sintered the SnO_2 particles, resulting in the final, robust ceramic structure shown in **Figure 4E**. This demonstrates the successful translation of a rheologically optimized paste into a well-defined, three-dimensional ceramic object.

The successful printing of phase-pure SnO_2 pieces represents a significant advance compared with traditional approaches, where foreign binders often introduce impurities or uncontrolled porosity. Compared to Qi et al. (2023) [25], who used DLP printing of Sb-doped SnO_2 electrodes to improve conductivity, the present work prioritises phase purity and structural integrity, aspects critical for catalytic applications where support composition must be tightly controlled. Moreover, unlike starch-assisted or porogen-based strategies for hierarchical porosity [22], the present approach establishes a clean baseline for subsequent incorporation of pore formers or mixed oxide chemistries.

4. CONCLUSION

In this work, we demonstrated a novel strategy for the additive manufacturing of phase-pure SnO_2 supports using direct ink writing (DIW) with a Pechini-derived reactive binder. The dual role of the binder, as both a rheological modifier and an *in-situ* oxide precursor, enabled the formulation of pastes with tailored viscoelastic properties while eliminating the presence of extraneous cations typically introduced by inert binders.

Rheological analyses identified the critical balance between yield stress and thixotropic recovery required for printability, with optimized formulations enabling extrusion within operational limits and maintaining structural fidelity during layer-by-layer deposition.

The successful fabrication of self-supporting SnO_2 pieces after calcination underscores the potential of reactive-binder formulations, inspired by the knowledge of nanotechnology fields, to bridge the gap between laboratory-scale catalyst powders and structured supports. Compared with conventional shaping routes, this approach provides superior chemical purity, geometric precision, and scalability. These characteristics are particularly relevant for catalytic applications, where support composition, porosity, and integrity strongly influence dispersion, stability, and activity of the active phase.

It is expected that this study, beyond proposing a reliable strategy for preparing pure-phase 3D ceramic pieces, establishes a foundation for future work exploring hierarchical porosity, mixed oxide systems, and integration into intensified catalytic reactor designs. As such, the methodology contributes both to the advancement of ceramic additive manufacturing and to the broader effort of engineering sustainable catalyst supports for applications in energy transition technologies.

5. ACKNOWLEDGEMENTS

The authors acknowledge the support of the Sao Paulo Research Foundation (FAPESP), grants 23/14214-4 and 24/13525-9. We gratefully acknowledge the support of the RCGI – Research Centre for Greenhouse Gas Innovation (23.1.8493.1.9), hosted by the University of São Paulo (USP) and sponsored by FAPESP – São Paulo Research Foundation (2020/15230-5) and Shell Brasil, as well as the strategic importance of the support given by ANP (Brazil's National Oil, Natural Gas and Biofuels Agency) through the R&DI levy regulation.

6. REFERENCES

(1) Gothe, M. L.; Figueredo, A. L.; Borges, L. R.; Ramos, R.; Peixoto, A. F.; Vidinha, P. High-Pressure Hydrogenation: A Path to Efficient Methane Production from CO2. *Methane* **2024**, *3* (1), 53–64. https://doi.org/10.3390/methane3010004.

(2) Podence Alves, C. A.; Palharim, P. H.; Pratto, B.; Da Silva, A. L.; Gouvêa, D.; Ramos, B. Photocatalytic Ammonia Synthesis from Nitrogen in Water Using Iron Oxides: Comparative Efficiency of Goethite, Magnetite, and Hematite. *J. Photochem. Photobiol. Chem.* **2025**, *460*, 116159. https://doi.org/10.1016/j.jphotochem.2024.116159.

(3) Palharim, P. H.; Gusmão, C.; Ramos, B.; Bento, R. T.; Pillis, M. F.; Teixeira, A. C. S. C. Highly Stable WO3-Ag-AgCl Films for Continuous Water Treatment Synthesized Using a New Low-Cost Ultrasonic Spray-Pyrolysis/Photoreduction Approach. *J. Environ. Chem. Eng.* **2024**, *12* (3), 112895. https://doi.org/10.1016/j.jece.2024.112895.

(4) Fernandes, M. H.; Ramos, B.; Da Silva, A. L.; Gouvêa, D. Chloride-Doped ZnO Thin Films Prepared by Spray Pyrolysis: Effects on Microstructural, Optical, and Photocatalytic Properties. *Micro Nanostructures* **2023**, *177*, 207550. https://doi.org/10.1016/j.micrna.2023.207550.

(5) Wu, C.-Y.; Lee, Y.-L.; Lo, Y.-S.; Lin, C.-J.; Wu, C.-H. Thickness-Dependent Photocatalytic Performance of Nanocrystalline TiO2 Thin Films Prepared by Sol–Gel Spin Coating. *Appl. Surf. Sci.* **2013**, *280*, 737–744. https://doi.org/10.1016/j.apsusc.2013.05.053.

(6) Ramos, B.; Couri, A. P.; Ookawara, S.; Costa Teixeira, A. C. S. Micro-Structured Packed Bed Reactors for Solar Photocatalysis: Impacts of Packing Size and Material on Light Harnessing. *Photochem. Photobiol. Sci.* **2019**, *18* (2), 577–582. https://doi.org/10.1039/c8pp00371h.

(7) An, K.; Alayoglu, S.; Musselwhite, N.; Plamthottam, S.; Melaet, G.; Lindeman, A. E.; Somorjai, G. A. Enhanced CO Oxidation Rates at the Interface of Mesoporous Oxides and Pt Nanoparticles. *J. Am. Chem. Soc.* **2013**, *135* (44), 16689–16696. https://doi.org/10.1021/ja4088743.

(8) Ivanova, S.; Pitchon, V.; Petit, C.; Caps, V. Support Effects in the Gold-Catalyzed Preferential Oxidation of CO. *ChemCatChem* **2010**, *2* (5), 556–563. https://doi.org/10.1002/cctc.200900302.

(9) Wu, S.; Xu, X.; Zhang, X.; Ji, Z.; Jia, X.; Wang, X. 3D-Printing Functional Ceramic for One-Step Fabrication of Pd/C Catalytic Reactor. *Addit. Manuf. Front.* **2024**, *3* (4), 200167. https://doi.org/10.1016/j.amf.2024.200167.

(10) Lewis, J. A. BINDER REMOVAL FROM CERAMICS. *Annu. Rev. Mater. Sci.* **1997**, *27* (1), 147–173. https://doi.org/10.1146/annurev.matsci.27.1.147.

(11) Oropeza, D.; Hart, A. J. Reactive Binder Jet Additive Manufacturing for Microstructural Control and Dimensional Stability of Ceramic Materials. *Addit. Manuf.* **2021**, *48*, 102448. https://doi.org/10.1016/j.addma.2021.102448.

(12) Barbosa, A. L.; De Oliveira Romano, R. C.; Bernardes, A. A.; Gouvêa, D. Rheological and Microstructural Characterization of Titania Pastes for Additive Manufacturing Using Polymeric Ceramic Precursor as Organic and Inorganic Binder. *Ceram. Int.* **2025**, *51* (17), 24072–24079. https://doi.org/10.1016/j.ceramint.2025.03.093.

(13) Li, Z. L.; Zhou, S.; Saiz, E.; Malik, R. Ink Formulation in Direct Ink Writing of Ceramics: A Meta-Analysis. *J. Eur. Ceram. Soc.* **2024**, *44* (12), 6777–6796. https://doi.org/10.1016/j.jeurceramsoc.2024.05.014.

(14) Inaba, M.; Murase, R.; Takeshita, T.; Yano, K.; Kosaka, S.; Takahashi, N.; Isomura, N.; Oh-ishi, K.; Yoshimune, W.; Tsuchiya, K.; Nobukawa, T.; Kodama, K. Synthesis of a Mesoporous SnO_2 Catalyst Support and the Effect of Its Pore Size on the Performance of Polymer Electrolyte Fuel Cells. *ACS Appl. Mater. Interfaces* **2024**, *16* (8), 10295–10306. https://doi.org/10.1021/acsami.4c01794.

(15) D'Arino, M.; Pinna, F.; Strukul, G. Nitrate and Nitrite Hydrogenation with Pd and Pt/SnO2 Catalysts: The Effect of the Support Porosity and the Role of Carbon Dioxide in the Control of Selectivity. *Appl. Catal. B Environ.* **2004**, *53* (3), 161–168. https://doi.org/10.1016/j.apcatb.2004.05.015.

(16) Anwar, M. Z.; Kim, D. J.; Kumar, A.; Patel, S. K. S.; Otari, S.; Mardina, P.; Jeong, J.-H.; Sohn, J.-H.; Kim, J. H.; Park, J. T.; Lee, J.-K. SnO2 Hollow Nanotubes: A Novel and Efficient Support Matrix for Enzyme Immobilization. *Sci. Rep.* **2017**, *7* (1), 15333. https://doi.org/10.1038/s41598-017-15550-y.

(17) Tai, L.; Anderson, H. U.; Lessing, P. A. Mixed-Cation Oxide Powders via Resin Intermediates Derived from a Water-Soluble Polymer. *J. Am. Ceram. Soc.* **1992**, *75* (12), 3490–3494. https://doi.org/10.1111/j.1151-2916.1992.tb04458.x.

(18) Sain, S.; Kar, A.; Patra, A.; Pradhan, S. K. Structural Interpretation of SnO_2 Nanocrystals of Different Morphologies Synthesized by Microwave Irradiation and Hydrothermal Methods. *CrystEngComm* **2014**, *16* (6), 1079–1090. https://doi.org/10.1039/C3CE42281J.

(19) Medvedovski, E. Tin Oxide-Based Ceramics of High Density Obtained by Pressureless Sintering. *Ceram. Int.* **2017**, *43* (11), 8396–8405. https://doi.org/10.1016/j.ceramint.2017.03.185.

(20) del-Mazo-Barbara, L.; Ginebra, M.-P. Rheological Characterisation of Ceramic Inks for 3D Direct Ink Writing: A Review. *J. Eur. Ceram. Soc.* **2021**, *41* (16), 18–33. https://doi.org/10.1016/j.jeurceramsoc.2021.08.031.

(21) Hossain, S. S.; Lu, K. Recent Progress of Alumina Ceramics by Direct Ink Writing: Ink Design, Printing and Post-Processing. *Ceram. Int.* **2023**, *49* (7), 10199–10212. https://doi.org/10.1016/j.ceramint.2023.01.143.

(22) Tabard, L.; Garnier, V.; Prud'Homme, E.; Courtial, E.-J.; Meille, S.; Adrien, J.; Jorand, Y.; Gremillard, L. Robocasting of Highly Porous Ceramics Scaffolds with Hierarchized Porosity. *Addit. Manuf.* **2021**, *38*, 101776. https://doi.org/10.1016/j.addma.2020.101776.

(23) Li, H.; Hou, W.; Zhang, Y. Rheological Properties of Aqueous Solution of New Exopolysaccharide Secreted by a Deep-Sea Mesophilic Bacterium. *Carbohydr. Polym.* **2011**, *84* (3), 1117–1125. https://doi.org/10.1016/j.carbpol.2010.12.072.

(24) Von Borries-Medrano, E.; Jaime-Fonseca, M. R.; Aguilar-Méndez, M. A. Tapioca Starch-Galactomannan Systems: Comparative Studies of Rheological and Textural Properties. *Int. J. Biol. Macromol.* **2019**, *122*, 1173–1183. https://doi.org/10.1016/j.ijbiomac.2018.09.067.

(25) Qi, G.; Yao, H.; Zeng, Y.; Chen, J. Preparation and Properties of Highly Loaded SnO2-Based Porous Electrodes by DLP 3D Printing. *J. Alloys Compd.* **2023**, *935*, 167941. https://doi.org/10.1016/j.jallcom.2022.167941.